Journal of
MATERIALS RESEARCH

The preparation of metal–polymer composite materials using ultrasound radiation: Part II. Differences in physical properties of cobalt–polymer and iron–polymer composites

S. Wizel, S. Margel, and A. Gedanken[a)]
Department of Chemistry, Bar-Ilan University, Ramat-Gan, Israel, 52900

T.C. Rojas and A. Fernández
Instituto de Ciencia de Materiales de Sevilla. Centro de Investigaciones Cientificas Isla de la Cartuja, Avda. Americo Vespucio s/n, 41092-Sevilla, Spain

R. Prozorov
Department of Physics, Bar-Ilan University, Ramat-Gan, Israel, 52900

(Received 18 May 1999; accepted 12 July 1999)

Composite materials containing amorphous iron embedded in poly(methylacrylate) or poly(methylmethacrylate) and amorphous cobalt embedded in poly(methylacrylate) were formed using a sonochemical method. The physical and thermal properties of the composite materials were probed. A significant difference in the solubility of the iron–poly(methylacrylate) and cobalt–poly(methylacrylate) in various solvents was observed. This difference is accounted for by the stronger interaction existing between the cobalt and the surrounding polymer. For iron–poly(methylacrylate) this interaction is weakened due to the formation of an iron complex.

I. INTRODUCTION

The preparation of polymer films containing dispersed metallic clusters or metallic colloids has been of great interest[1–7] because of both its practical and fundamental importance. The potential use of colloidal iron dispersions in polymers lies in magnetic recording devices and pigments.[7] The application of polymers containing dispersed metallic clusters to catalysis has been the motivation for all electrochemical studies.[1–6] Apart from their useful catalytic activity toward technologically important substrates, these polymers provide unique opportunities for exploring novel types of catalyst-support interactions. The two main techniques employed in the preparation of the metal–polymer composites are electrochemical[8,9] and thermolysis[10] techniques.

Successful attempts to disperse iron and cobalt in various polymers have been reported.[10–13]

The application of high-intensity ultrasound radiation in polymer chemistry has been an active research area.[14–16] The main advantages of ultrasonic polymerization are the absence of initiator, the low temperature range in which the reaction take place, and the possibility of bulk polymerization.

The propagation of ultrasound waves through a fluid causes the formation of cavitation bubbles.[17] The collapse of these bubbles, described as an implosion in the hot-spot theory, is the origin of extreme local conditions: high temperatures (5000–25,000 K) and high pressures (1000 atm).[17] The cooling rates obtained during the collapse are greater than 10^7 K/s.[18,19] These high cooling rates were utilized by Suslick and coworkers in sonicating iron pentacarbonyl as a neat liquid or in solution,[18,19] to prepare amorphous iron nanoparticles. Suslick *et al.* also prepared amorphous cobalt[20] and an amorphous Fe–Co alloy.[21] We prepared amorphous Ni,[22] amorphous Fe_2O_3[23] amorphous Mo_2O_5,[24] and amorphous Cr_2O_3 and Mn_2O_3,[25] all with nanometer-size particles.

The first polymerization reaction synthesis using ultrasound radiation was that of acrylonitrile in aqueous solution.[26] Kruus, and coworkers, studied the polymerization of nitrobenzene,[27] methylmethacrylate,[28,29] and other monomers as well.[29] Price *et al.* studied the polymerization of methyl methacrylate.[30,31] We recently reported[32] on the preparation of composite materials containing polymethylacrylate and amorphous iron nanoparticles using ultrasound radiation.

In this investigation we extend our sonochemical preparation to methylmethacrylate, and preparation of dispersed cobalt. The solubility properties of the cobalt-containing composites in various solvents, were different from those of the iron–polymer composites. We propose

a)Address all correspondence to this author.
e-mail: gedanken@mail.biu.ac.il

an explanation for the solubility properties by investigating the molecular weight, differential scanning calorimetry (DSC), thermogravimetrical analysis (TGA), x-ray photoelectron spectroscopy (XPS), and magnetic properties of the composite materials.

II. EXPERIMENTAL

The amorphous metal (iron or cobalt) nanoparticles were prepared following the procedure described by Suslick *et al.*[18–20] and Grinstaff *et al.*[19] The precursors were iron pentacarbonyl, for the amorphous iron, and cobalt tricarbonyl nitrosyl for the amorphous cobalt. The dried amorphous metal powder was introduced into the sonication cell without exposure to air. Thirty-five milliliters of a 5.5-M solution of a distilled methylacrylate (MA) monomer in dry N,N′-dimethylformamide (DMF) were mixed with various amounts of amorphous metal nanoparticles. The amounts of the metal powder were changed from 1.4 to 5.7 g l^{-1}. The solution was sonicated (Sonics and Materials, VC-600, 20 kHz, 100 W/cm^2) for 90 min under argon (100 ml/min, 1 atm) using a cooling bath (−90 °C, Julabo FT 901). The sonication cell was kept in dark by wrapping it with aluminum foil to avoid photopolymerization. The sonication product was a colloidal solution that was stable for at least a month. The polymer was precipitated from the colloidal solution by adding, under nitrogen atmosphere, an excess of cold methanol at the end of the sonication. The precipitate was vacuum dried at room temperature overnight and then subjected to various examinations. The same procedure was followed for the preparation of Fe–poly(methylmethacrylate) composite. For the cobalt composites, we succeeded only in preparing the cobalt–poly(methylacrylate), but could not obtain the corresponding methylmethacrylate composite. Elemental analysis for iron and cobalt contents was carried out by an inductively coupled plasma–atomic emission spectroscopy (ICP-AES) instrument (Spectroflame, Spectro), using Merck standards.

The determination of the polymer's molecular weight (MW) was carried out using a gel permeation chromatography (GPC; Thermo Separation Products, AS100) instrument using poly(metylmethacrylate) PMMA standards (Pressure Chemicals) for calibration. The composite material was treated in the following way prior to its introduction into the GPC instrument. The material was dissolved in acetone, and the untrapped metal was precipitated and removed from the solution. In the cobalt–poly(methylacrylate) composite case, the polymer was stirred and heated in acetone using sonication bath for 1 h in order to dissolve it in the acetone solvent. To the resulting acetone solution, an excess of cold methanol was added, precipitating the polymer. The polymer was vacuum dried overnight, then dissolved in chloroform (10 mg/ml), and injected into the GPC instrument. The column used was phenogel heated to 30 °C. A Shodex RI-71 refractive index detector was employed in these experiments.

Transmission electron microscopy (TEM) examination of the samples was carried out in a Philips CM200 microscope operated at 200 kV. The powdered samples were dispersed in ethanol by sonication and dropped on a conventional carbon-coated copper grid. Metal–polymer composite samples were prepared by the epoxy embedding technique, followed by ultramicrotome cutting.

The size distribution of the dispersed metallic particles in the polymer was followed by the dynamic light scattering (DLS) technique, using a Coulter N4 Plus instrument. The as-prepared colloidal solution was measured for its particles size without further treatment.

Magnetization loops were measured at room temperature, using an Oxford Instrument vibrating sample magnetometer (VSM).

The TGA measurements were carried out under nitrogen on a Mettler TC11 TA processor in a temperature range of 25–900 °C in a heating rate of 10 °/min.

The DSC spectra were recorded under argon using a Mettler DSC 25 (TC15 TA controller) instrument in the temperature range of 25–500 °C, in a heating rate of 10 °/min.

XPS spectra were collected on an ESCALAB 210 Spectrometer (VG). The instrument was operated in the constant pass energy mode, with a value of 50 eV, using Al K_α as excitation source. Calibration of the spectra was done at the C1s main peak at 284.6 eV. A second peak in the spectra is due to carbon bounded to oxygen in the polymer.

Absorption spectra were measured on ultraviolet-visible (UV-VIS) double-beam spectrophotometer (Cary 1E, Varian). Fifty milligrams of amorphous metal were mixed with 10 ml of distilled methylacrylate for 5 min and then measured for its absorption versus distilled methylacrylate. The same procedure was carried out for dried DMF.

III. RESULTS AND DISCUSSION

The solubility of the iron and cobalt composites was examined in various solvents. While the iron–poly(methylacrylate) composite (FePMA) and iron–poly(methylmethacrylate) composite (FePMMA) dissolved in chloroform, acetone, and toluene at room temperature, the corresponding cobalt–poly(methylacrylate) composite (CoPMA) was insoluble in these solvents at room temperature. At elevated temperatures (45 °C), a dissolution of CoPMA in these solvents was observed.

The most distinctive difference between the FePMA and CoPMA lies in their solubility patterns. To account

for this difference, we probed the possibility of complex formation between the amorphous metal and the methylacrylate or the DMF solvent. Indeed, we found that the amorphous iron forms a colored complex with these two reactants, while cobalt does not form corresponding complexes. Evidence for the formation of iron complexes with the MA and the DMF is manifested in the corresponding absorption spectra, which show a broad structureless continuum peaked at 500 and 542 nm, respectively. In Figs. 1 and 2 we present the absorption spectra of the Fe and Co nanoparticles reacting with MA (Fig. 1) and with DMF (Fig. 2). The formation of iron–DMF complex has been previously reported[33] in the literature, whereas no reports exist for iron–MA. Since the amorphous iron nanoparticles are much more reactive than the nanocrystalline iron,[34] this complex appears only when amorphous iron reacts with MA. We explain the solubility differences as follows. The iron agglomerates form chemical bonds with the DMF and MA ligands, thus screening and weakening the direct interaction between the metal and the polymer. In the case of cobalt, the cobalt interacts directly with the polymer. When the composite material is dissolved in the various solvents, the stronger interactions between the poly(methylacrylate)

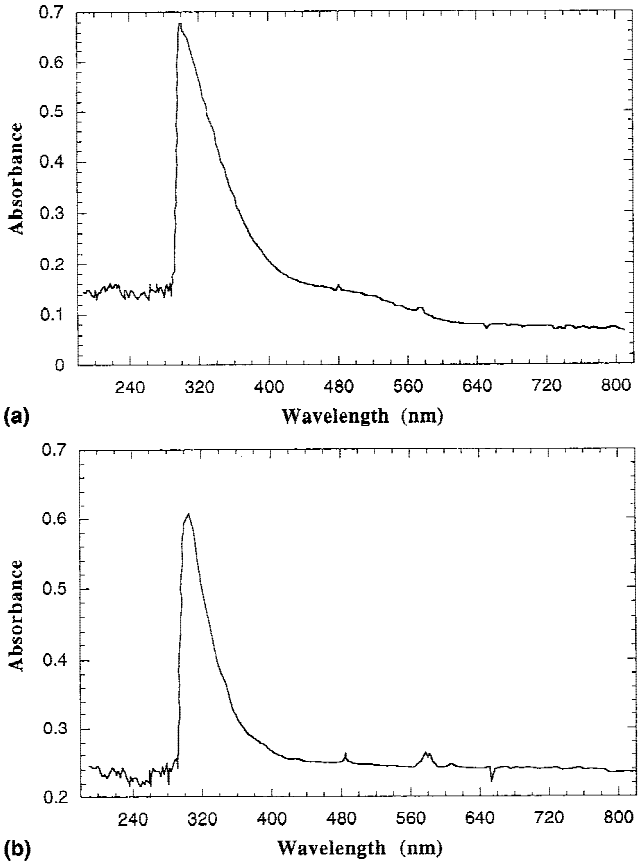

FIG. 1. UV-VIS absorption spectra of methylacrylate with (a) amorphous Fe and (b) amorphous Co versus methylacrylate.

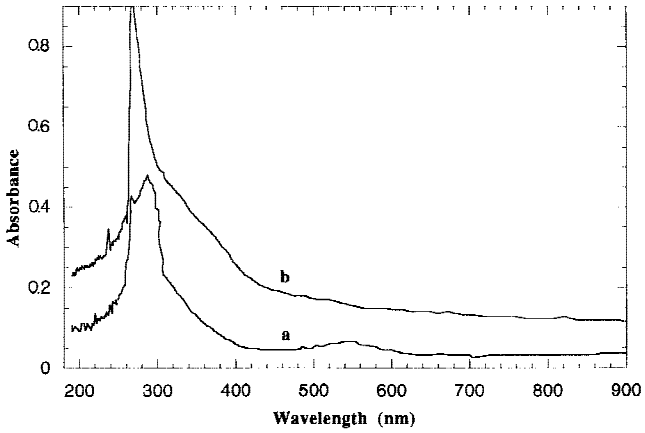

FIG. 2. UV-VIS absorption spectra of DMF with (a) amorphous Fe and (b) amorphous Co versus DMF.

and the cobalt metal are not easily replaced by the solvent molecules, and these bonds remain intact. In the iron case, where the interaction is much weaker, the solvent molecules succeed in breaking the chemical bonds between the iron and the PMA and dissolve the composite. This theory is also supported by other methods and will be detailed later.

A. Chemical analysis

In Table I we present the results of chemical analysis comparing the metal content of the FePMA with that of CoPMA. It is clear that iron is more favorably introduced into the polymeric material. This is due to the complex formation of the Fe–DMF and Fe–MA, which causes the introduction of more metallic material in the composite.

B. Molecular weight measurements

The MW of the various polymers and composites as a function of the metal-to-monomer weight ratio are presented in Table I. The table contains the data of the composites: FePMA, CoPMA, FePMMA, and the polymers: poly(methylacrylate) and poly(methylmethacrylate) which were prepared by the same procedure as the composites but do not contain any metal (PolyMA and PolyMMA, respectively).

The general features observed in the table are that the molecular weights of the CoPMA are always larger than those of the corresponding FePMA. This comparison is made for equal amounts of starting materials. The second observation is that the larger the amount of the metal, the smaller the molecular weight of the PMA. The opposite is observed for the FePMMA, where a larger molecular weight is obtained for higher amounts of iron clusters. We explain this phenomenon as due to the presence of the oxidized iron, especially Fe^{+3}. These ions are accelerating the polymerization of the methylmethacrylate,[35] and a higher amount of metal will favor a higher mo-

TABLE I. Metal concentrations, molecular weights, and particles size distribution for the various polymers and composites.

	Metal in starting solution (% by weight)	Metal in composite polymer (% by weight)	Mw	Size (nm)	S.D. (nm)
PolyMA	…		307,000		
	0.30	5.4	167,000	558.3	352.8
FePMA	0.60	19.2	152,000	373.4	139.2
	1.20	22.0	127,000	219.9	42.0
	0.30	2.1	228,000	152.4	18.7
CoPMA	0.60	7.8	215,000	157.6	25.9
	1.20	19.1	187,000	161.5	22.2
PolyMMA	…		70,000		
	0.30		79,000	595.5	219.9
FePMMA	0.61		87,000	310.4	92.0
	1.22		249,000	253.7	47.8

lecular weight polymer. The presence of an oxidized iron is supported by XPS and x-ray absorption near-edge spectroscopy (XANES) measurements and will be discussed further on. The explanation for the opposite behavior encountered for CoPMA and FePMA, where a larger amount of the metal is causing the decrease of the molecular weight of the polymer, is associated with a stronger interaction between the Co and Fe and the polymeric radical. This decelerates the growth of the polymeric chain.

It is worth mentioning again that we could not detect the formation of the corresponding CoPMMA. The reason for that probably has to do with the interaction of the cobalt with the PMMA radical chain, which inhibits the polymerization process.

C. DLS

The DLS of the as-prepared solutions (Table I) which demonstrates the sizes of the individual polymer spheres shows that the particle sizes are dependent on the amount of the metal trapped in the polymer. For the FePMA and FePMMA, it was observed that the larger the amount of the metal introduced into the polymer, the smaller the particles size and the narrower is the distribution [demonstrated by the standard deviation (S.D.)]. Since we have found that iron oxide is present on the surface of the iron particles, we attribute the stabilization of the colloidal solution to the charge on the surface area of the particles, resulting in a smaller particles.[36]

D. TEM

TEM studies of the cobalt and iron powders show that the cobalt particles formed are smaller than the iron particles, having typical particle sizes of 10–30 nm and 50–90 nm, respectively; this is due to the higher concentration of the iron pentacarbonyl solution than the cobalt tricarbonyl nitrosyl solution, which were used in the preparation of the amorphous metal.[37] Low-magnification images of the composite materials, CoPMA and FePMA, containing 0.6 wt% metal in the starting solution (CoPMA0.6 and FePMA0.6, respectively), are presented in Fig. 3. For the iron sample [Fig. 3(b)], the metal particles appear agglomerated, leading to many regions of intact polymer, free of metal.

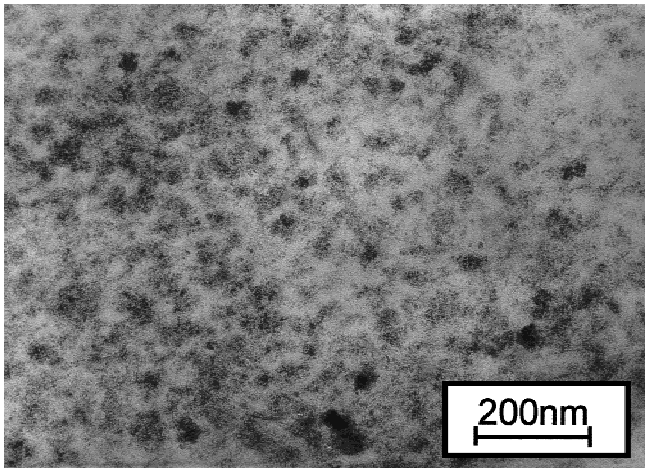

(a)

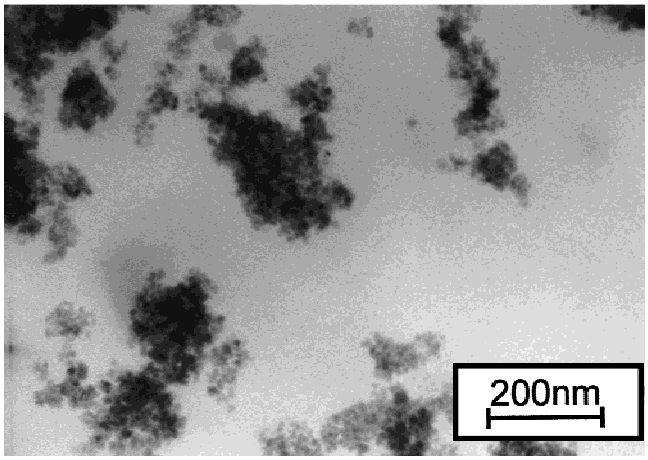

(b)

FIG. 3. Low-magnification TEM images of the (a) CoPMA0.6 and (b) FePMA0.6 samples.

In the case of cobalt [Fig. 3(a)], the metal appears very well dispersed in the polymer, leading to a high polymer–metal interaction. The same results have been found for composite materials with a higher metal content (FePMA1.2 and CoPMA1.2).

E. Magnetic properties

In Fig. 4 we present the magnetic measurements results of FePMMA [Fig. 4(a)] which shows superparamagnetic behavior due to single-domain particles. The FePMMA does not show saturation of the magnetization and also lacks hysteresis in its magnetization loops. The same behavior is detected for the CoPMA [Fig. 4(b)] sample. The magnetization values measured for the cobalt particles were always smaller than those of the iron. This is also true for the bulk magnetization.[38]

F. TGA

In Fig. 5 we present the TGA curves of FePMA0.3 [Fig. 5(a)], CoPMA0.3 [Fig. 5(b)], and PolyMA [Fig. 5(c)]. The inflection points of the three composites were 349, 410, and 409 °C, respectively. This sharp drop in weight is assigned to the decomposition of the polymer. While CoPMA and PolyMA decompose over a narrow temperature range and show sharp slopes in their weight loss, the corresponding FePMA changes its slope at about 500 °C and continues to lose weight up to 900 °C. This high-temperature weight loss is attributed to the rupture of the Fe–DMF and Fe–MA complexes bonds. The large temperature range of this weight loss is interpreted as being due to the wide size distribution of the agglomerated iron particles and the formation of the complexes around each particle.

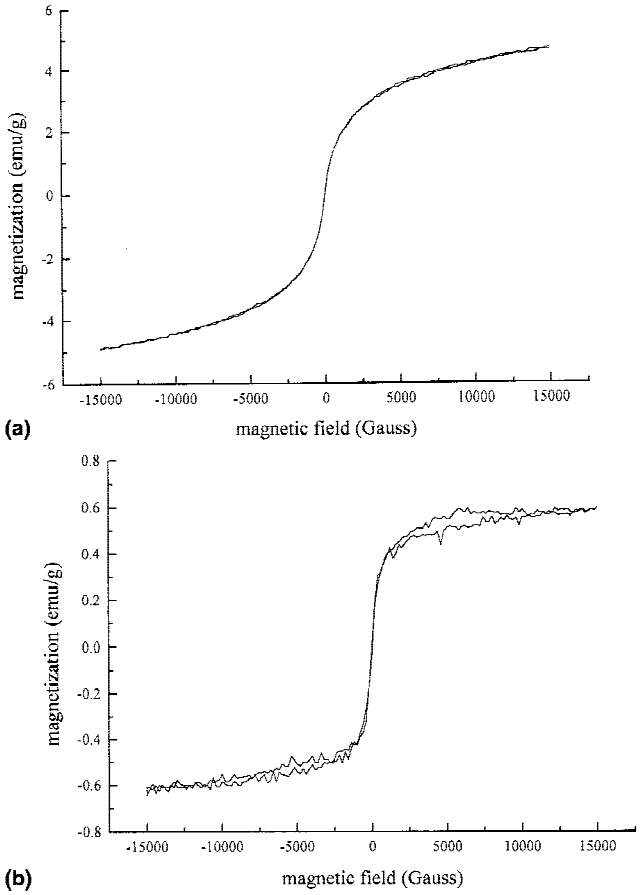

FIG. 4. Room-temperature magnetization loops of (a) FePMMA1.22 and (b) CoPMA1.2.

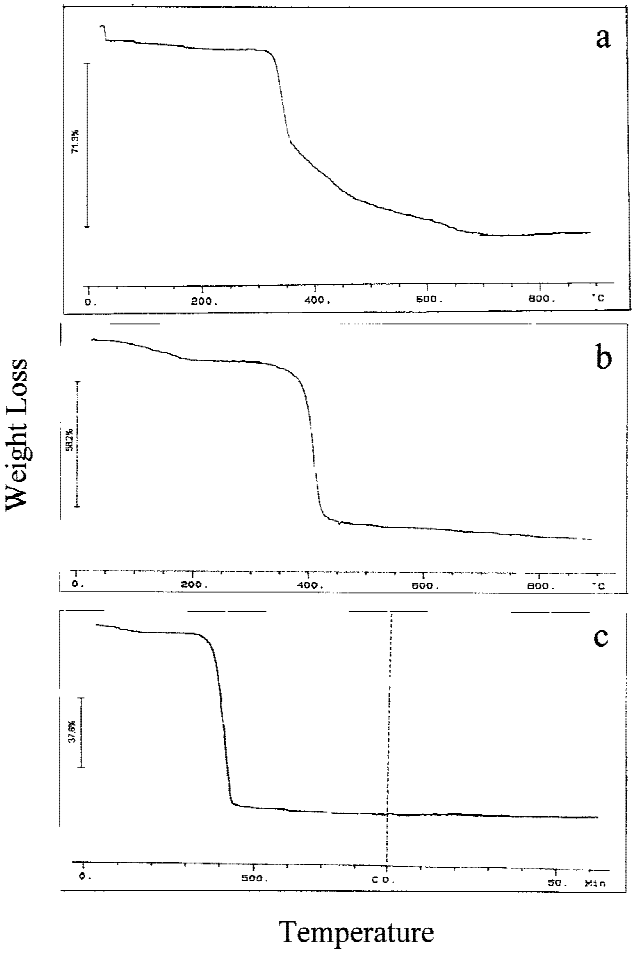

FIG. 5. TGA spectra of (a) FePMA0.3, (b) CoPMA0.3, and (c) PolyMA. The spectra were measured at a heating rate of 10 °C/min. In the case of (c) PolyMA an isotherm was measured for 60 min in a temperature of 900 °C.

G. DSC

In Fig. 6, we present the DSC of the FePMA0.3 [Fig. 6(a)], CoPMA0.3 [Fig. 6(b)], and PolyMA [Fig. 6(c)]. In all cases we have observed an endothermic peak at almost the same temperatures as the inflection points in the TGA spectra (±6 °C). We interpret the lower decomposition temperature of the as-compared with the CoPMA and PolyMA as due to the different

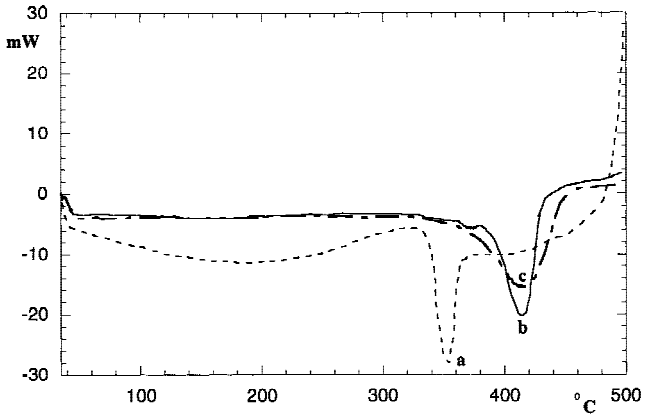

FIG. 6. DSC spectra of (a) FePMA0.3, (b) CoPMA0.3 and (c) PolyMA.

arrangement and packing of the polymer chains in the FePMA as a result of the complexes formed between the iron and the methylacrylate or the DMF. Cobalt does not form these complexes and therefore the arrangements of the polymer chains are unchanged as compared with PolyMA.

H. XPS

The XANES region of the x-ray absorption spectroscopy (XAS) spectra contain information about oxidation states and local structure around the absorbing atom. Although multiple scattering calculations can be carried out to simulate the XANES spectra, a fingerprint technique can also be used to obtain conclusions from this data just by comparison with reference samples.[39] Following this method we plotted in Fig. 7 the Co and Fe K edges spectra for samples CoPMA0.6 and FePMA1.2 and compared them with the spectra of the metallic Co and Fe foils as well as α–Fe_2O_3 and CoO reference samples, respectively.

The first region in the spectra corresponds to a low-energy shoulder before the edge threshold at around 7711 and 7113 eV for Co and Fe respectively. This shoulder is usually attributed to the $1s \rightarrow 4d$ transition, which, in perfect Oh symmetry, is strictly dipole forbidden. However, due to the mixing of *p*- and *d*-like states, this feature is visible. While the energy position of this transition is found to be not very sensitive to the oxidation state and local structure of the iron and cobalt atoms, the intensity of the peak is strongly dependent on it, as demonstrated in Fig. 7. The second region of the spectra corresponds to the sharp rise in absorption associated with the excitation of the 1*s* electron into the ionization continuum. In the third region, a few eV above the threshold, the photoelectron wavelength is very long, and the photoelectron mean free path is large. Therefore, in the near region above the edge, the final states of the photoelectron should be described as unoccupied bands close to the Fermi level. Because of the fully screened core hole, the edge spectrum probes the unoccupied density of states of the ground state of the material. In this sense, the strong absorption at about 7728 and 7130 eV for cobalt and iron, respectively, can be assigned as the transition of an electron from 3*d* to the 4*p* energy level and is clearly dependent on the oxidation state of the metal. From a comparison of the above-described features in the spectra for the metal–polymer composite materials and the metal and oxide reference compounds, it is clear that oxidized iron and cobalt atoms are present at the surface area. Since the percentage of these surfacial atoms is high for nanoparticles, we conclude that despite all the precau-

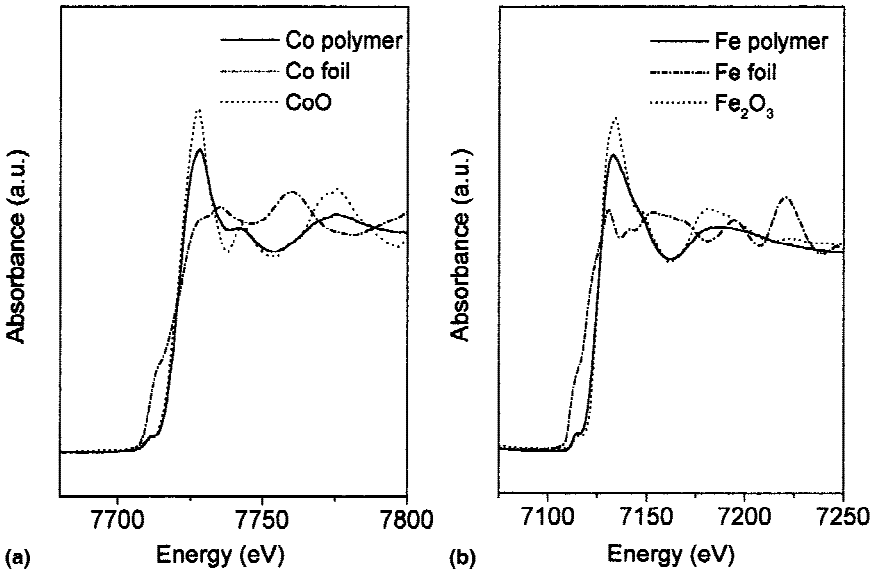

FIG. 7. (a) Cobalt and (b) iron K-edge XANES spectra of CoPMA0.6 and FePMA1.2 samples in comparison with commercial Co and Fe foils and CoO and α–Fe_2O_3 reference samples.

tions taken in shipping and handling the samples, the small core of zero-valent metal atoms is definitely coated with an amorphous oxide layer.

In Fig. 8, we plotted the spectra for powdered Co and Fe amorphous samples and for Co and Fe polymer composites, respectively. It is interesting to see how, in the case of iron, both spectra are very similar, indicating that the oxidation degree of iron has not been changed by its interaction with the polymer in which it is dispersed. The similarity of both spectra also indicates the absence of any interaction between the iron and the polymer. In the case of cobalt, we observe a certain reduction in the average oxidation state for the polymer composite sample, in comparison with the free powder, as stated for the decrease in intensity of the peak at 7728 eV. This can be attributed either to the nature of the Co–polymer interaction or, what is also likely, to a preservation of the cobalt metal against oxidation inside the polymeric matrix. It is also our experience that when amorphous cobalt is left in the open air for a month the x-ray diffraction did not show any evidence for its oxidation.

XPS data were recorded for FePMA1.2 and CoPMA1.2. In these samples, the spectra are dominated by carbon and oxygen photoelectron peaks corresponding to the polymer, as expected for metal particles embedded in the polymeric matrix. In the case of the CoPMA samples, the Co2*p* signal is almost undetectable. In the case of the FePMA sample (Fig. 9), the Fe2*p* photoelectron peak could be recorded after a very long acquisition time, to improve the signal-to-noise ratio. The Fe2*p* spectrum reveals three main peaks, the doublet $2p_{3/2}$ and $2p_{1/2}$ at 710.5 and 723.9 eV and the shake-up resonance transition of the $2p_{3/2}$ at around 718 eV. The position of the main doublet is compared with the energies of the corresponding photoelectrons in Fe^0, Fe^{+2} and Fe^{+3}. The literature value[40] for the $2p_{3/2}$ peak in Fe^0 is 706.7, while for oxidized iron the corresponding value is 710.7 eV for Fe^{+3} and 709.6 for Fe^{+2}.[38] The comparison with the values obtained for FePMA indicates clearly that the iron is oxidized. However, the low intensity of the shake-up satellite at around 718 eV, observed in this sample, is congruent with a major presence of Fe^{+2} species. The intensity of this satellite has been demonstrated to be more important for Fe^{+3} species.[41]

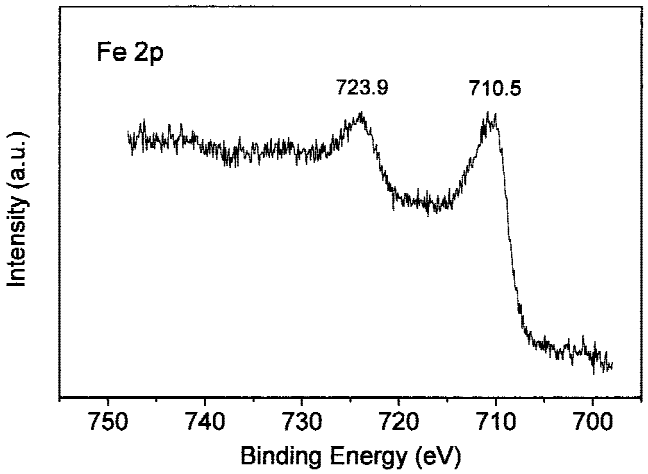

FIG. 9. Fe2*p* photoelectron spectrum of the FePMA 1.2 sample.

This interpretation is in agreement with the TGA results, which clearly show the decomposition of the composite material at lower temperatures for the FePMA than for the CoPMA.

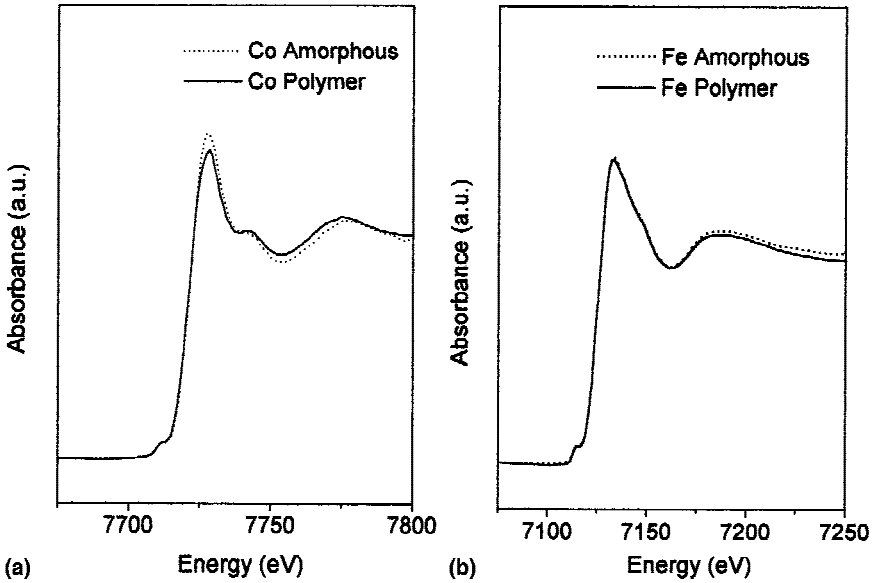

FIG. 8. Co and Fe K-edge XANES spectra of amorphous powdered cobalt and iron compared with the spectra of (a) CoPMA0.6 and (b) FePMA1.2 samples, respectively.

In the same way, we can account for the differences observed in the XANES results, where the spectra of the Fe and the FePMA samples are the same, while a reduction in the average oxidation state is detected for cobalt in the CoPMA, as compared with the spectrum of pure cobalt powder. The unscreened cobalt atom strongly interacts with the polymer. The backdonation of nonbonding electrons on the oxygen atom of the MA causes the partial reduction of the cobalt atom. The shielding by the ligands of the central atom, Fe, from the surrounding polymer, on the other hand, prevents any change in its oxidation number.

ACKNOWLEDGMENTS

Professor A. Gedanken thanks the research authorities of Bar-Ilan University for their financial help. He also thanks the Israel Academy of Science and the Bat-Sheba de Rotshield foundation for supporting synchrotron radiation experiments. We thank Professor Y. Yeshurun for extending the facilities of the National Center for Magnetic Measurements at the Department of Physics, Bar-Ilan University. We also thank Dr. S. Hochberg for editorial assistance. One of us, Professor S. Margel, thanks the Minerva Foundation and the Israeli Ministry of Science for financial support. T.C. Rojas and A. Fernández thank the DGES for financial support (0863-C02-02).

REFERENCES

1. R.N. Dominy, N.S. Lewis, J.A. Bruce, D.C. Bookbinder, and M.S. Wrighton, J. Am. Chem. Soc. **104,** 467 (1982).
2. J.A. Bruce, T. Murahashi, and M.S. Wrighton, J. Phys. Chem. **86,** 1552 (1982).
3. W.H. Kao and T. Kuwana, J. Am. Chem. Soc. **106,** 473 (1984).
4. D. Weisshaar and T. Kuwana, J. Electroanal. Chem. **163,** 395 (1984).
5. D.E. Bartak, B. Kazee, K. Shimazu, and T. Kuwana, Anal. Chem. **58,** 2756 (1986).
6. M. Kost, D.E. Bartak, B. Kazee, and T. Kuwana, Anal. Chem. **60,** 2379 (1988).
7. C.H. Griffiths, M.P. O'Horo, and T.W. Smith, J. Appl. Phys. **50,** 7108 (1979).
8. C.S.C. Bose and K. Rajeshwar, J. Electroanal. Chem. **333,** 235 (1992).
9. C.C. Chen, C.S.C. Bose, and K. Rajeshwar, J. Electroanal. Chem. **350,** 161 (1993).
10. J.R. Thomas, J. Appl. Phys. **37,** 2914 (1966).
11. T.W. Smith and D. Wychick, J. Phys. Chem. **84,** 1621 (1980).
12. R. Tannenbaum, C.L. Flenniken, and E.F. Goldberg, J. Polym. Sci., Part B: Polm. Phys. **28,** 2421 (1990).
13. L.M. Bronstein, E.Sh. Mirzoeva, P.M. Valetsky, S.P. Soand, and R.A. Register, J. Mater. Chem. **5,** 1197 (1995).
14. G.J. Price, Adv. Sonochem. **1,** 231 (1990).
15. O. Lindstrom and O. Lamm, J. Phys. Colloid. Chem. **55,** 1139 (1951).
16. A. Henglein, Macromol. Chem. **14,** 15 (1954).
17. K.S. Suslick, *Ultrasound: Its Chemical, Physical and Biological Effects* (VCH Publishers, 1988), Chap. 4.
18. K.S. Suslick, S-B. Choe, A.A. Cichowlas, and M.W. Grinstaff, Nature **353,** 414 (1991).
19. M.W. Grinstaff, A.A. Cichowlas, S.B. Choe, and K.S. Suslick, Ultrasonics **30,** 168 (1992).
20. K.S. Suslick, T. Hyeon, M. Fang, and A.A. Cichowlas, in *Molecularly Designed Nanostructured Materials,* edited by K.E. Gonsalves, G.M. Chow, and R.C. Cammarata (Mater. Res. Soc. Symp. Proc. **351,** Pittsburgh, PA, 1994), pp. 201–206.
21. K.S. Suslick, T. Hyeon, M. Fang, and A.A. Cichowlas, in *Molecularly Designed Nanostructured Materials,* edited by K.E. Gonsalves, G.M. Chow, and R.C. Cammarata (Mater. Res. Soc. Symp. Proc. **351,** Pittsburgh, PA, 1994), pp. 443–448.
22. Yu. Koltypin, X. Cao, G. Kataby, R. Prozorov, and A. Gedanken, J. Non-Cryst. Solids **201,** 159 (1996).
23. X. Cao, R. Prozorov, Yu. Koltypin, G. Kataby, I. Felner, and A. Gedanken, J. Mater. Res. **12,** 402 (1997).
24. N.A. Dhas and A. Gedanken, J. Phys. Chem. B **101,** 9495 (1997).
25. N.A. Dhas, Yu. Koltypin, and A. Gedanken, Chem. Mater. **9,** 3159 (1997).
26. D.J. Donaldson, M.D. Farrington, and P. Kruus, J. Phys. Chem. **83,** 3130 (1979).
27. P. Kruus and T.J. Patraboy, J. Phys. Chem. **89,** 3379 (1985).
28. P. Kruus, Ultrasonics **21,** 201 (1983).
29. P. Kruus, M. O'Neill, and D. Robertson, Ultrasonics **28,** 304 (1990).
30. G.J. Price, D.J. Norris, and P.J. West, Macromolecules **25,** 6447 (1992).
31. G.J. Price and A.M. Patel, Polymer **33,** 4423 (1992).
32. S. Wizel, R. Prozorov, Y. Cohen, D. Aurbach, S. Margel, and A. Gedanken, J. Mater. Res. **13,** 211 (1998).
33. R. Schmid, K. Kirchner, and F.L. Dickert, Inorg. Chem. **27,** 1530 (1988).
34. G. Kataby, T. Prozorov, Yu. Koltypin, H. Cohen, C.N. Sukenik, A. Ulman, and A. Gedanken, Langmuir **13,** 6151 (1997).
35. A. Dutta, P.K. Mahato, and N.N. Dass, Eur. Polym. J. **27,** 465 (1991).
36. R.J. Hartman, *Colloid Chemistry* (Houghton Mifflin Company, 1947), p. 260.
37. X. Cao, G. Kataby, Yu. Koltypin, R. Prozorov, and A. Gedanken, J. Mater. Res. **10,** 2952 (1995).
38. D.L. Leslie-Pelecky and R.D. Rieke, Chem. Mater. **8,** 1770 (1996).
39. A. Bianconi, in *X-Ray Absorbtion: Principles, Applications, Techniques of EXAFS, SEXAFS and XANES,* edited by D.C. Konigsberger and R. Prins (John Wiley & Sons, New York, 1988) pp. 573–662.
40. *Practical Surface Analysis. Volume 1: Auger and X-Ray Photoelectron Spectroscopy,* edited by D. Briggs and M.P. Seah (John Wiley, New York, 1990).
41. Y.J. Kim, Y. Gao, and S.A. Chambers, Surf. Sci. **371,** 358 (1997).